John von Neumann Institute for Computing


# Massively Parallel Direct Numerical Simulation of Turbulent Combustion

Marc Lange, Jürgen Warnatz

published in

*NIC Symposium 2001, Proceedings*,
Horst Rollnik, Dietrich Wolf (Editor),
John von Neumann Institute for Computing, Jülich,
NIC Series, Vol. **9**, ISBN 3-00-009055-X, pp. 419-429, 2002.



http://www.fz-juelich.de/nic-series/volume9

# Massively Parallel Direct Numerical Simulation of Turbulent Combustion

**Marc Lange**[1,2] **and Jürgen Warnatz**[1]

[1] Interdisciplinary Center for Scientific Computing (IWR)
Heidelberg University, INF 368, 69120 Heidelberg, Germany

[2] High-Performance Computing-Center Stuttgart (HLRS)
Stuttgart University, Allmandring 30, 70550 Stuttgart, Germany
*E-mail: lange@hlrs.de*

A parallel code for the direct numerical simulation of turbulent reactive flows is presented. Detailed models are used for chemical kinetics and molecular transport. The performance of this code on the Cray T3E is briefly discussed. Several application examples regarding non-premixed and premixed turbulent combustion are given.

## 1 Introduction

Combustion processes are important for a wide range of applications like automotive engines, electrical power generation, and heating. This leads to an enourmous interest in improved predictive methods to aid the design of practical combustion systems with improved economy and reduced pollutant emissions. In most of these applications the reactive system is turbulent and the reaction progress is influenced by turbulent fluctuations and mixing in the flow. Due to the broad spectrum of length and time scales apparent in turbulent reactive flows, a direct numerical simulation (DNS), i. e. the direct solution of the equations describing the dynamics of reacting gas mixtures as given in Sect. 2, of most practical combustion devices will remain computationally prohibitive for the near future. The simulation of such systems must therefore continue to be done by the formulation and solution of model equations involving some form of averaging[1]. The nonlinear equations of fluid mechanics when averaged contain additional unknown quantities, the Reynolds stresses, so the averaged equations must be supplemented by appropriate model expressions before a closed system of equations can be obtained. The coupling between the chemical kinetics and fluid dynamics constitutes one central problem in turbulent combustion modeling[2].

During the last couple of years, DNS have become an important tool to study turbulent combustion at a fundamental level. The detailed information about turbulence-chemistry interactions provided by DNS has been extremely valuable in the development and validation of turbulent combustion models[3]. However, many of the DNS carried out so far have used simple one-step reaction mechanisms and/or oversimplified models for molecular transport. It has been shown[4,5] and will also become clear from the applications presented later in this paper that several important effects cannot be captured by simulations with such oversimplified models. By making efficient use of the computational power provided by parallel computers, it is possible to perform DNS of reactive flows using detailed chemical reaction mechanisms at least in two spatial dimensions[6,7]. Nevertheless, computation time is still the main limiting factor for the DNS of reacting flows, especially in the case of using realistic models for chemical kinetics and molecular transport.

## 2 Mathematical Model for Reactive Flows

Chemically reacting flows can be described by a set of coupled partial differential equations expressing the conservation of total mass, the masses of the $N_\mathrm{S}$ chemical species, momentum, and energy[8]. Employing tensor notation, where no summation over the index $\alpha$ which denotes the chemical species is performed, these equations can be written as

$$\frac{\partial \varrho}{\partial t} + \frac{\partial(\varrho u_i)}{\partial x_i} = 0 \quad , \tag{1}$$

$$\frac{\partial(\varrho Y_\alpha)}{\partial t} + \frac{\partial(\varrho Y_\alpha u_i)}{\partial x_i} = -\frac{\partial j_{\alpha i}}{\partial x_i} + M_\alpha \dot{\omega}_\alpha \quad (\alpha = 1, \ldots, N_\mathrm{S}), \tag{2}$$

$$\frac{\partial(\varrho u_i)}{\partial t} + \frac{\partial(\varrho u_i u_j)}{\partial x_j} = \frac{\partial \tau_{ij}}{\partial x_j} - \frac{\partial p}{\partial x_i} \quad , \tag{3}$$

$$\frac{\partial e_\mathrm{t}}{\partial t} + \frac{\partial((e_\mathrm{t} + p)u_i)}{\partial x_i} = \frac{\partial(u_i \tau_{ji})}{\partial x_i} - \frac{\partial q_i}{\partial x_i} \quad . \tag{4}$$

Herein, $\varrho$ denotes the density and $\vec{u}$ the velocity. $Y_\alpha$, $\vec{j}_\alpha$ and $M_\alpha$ are the mass fraction, diffusion flux, and molar mass of the species $\alpha$. $\tau_{ij}$ denotes the viscous stress tensor and $p$ the pressure, $\vec{q}$ is the heat flux and $e_t$ is the total energy given by

$$e_\mathrm{t} = \varrho \left( \frac{u_i u_i}{2} + \sum_{\alpha=1}^{N_\mathrm{S}} h_\alpha Y_\alpha \right) - p \quad , \tag{5}$$

where $h_\alpha$ is the specific enthalpy of the species $\alpha$. The term $\dot{\omega}_\alpha$ on the right-hand sides of Eq. (2) is the chemical production rate of the species $\alpha$, which is given as the sum of the formation rates in all $N_\mathrm{R}$ elementary reactions,

$$\dot{\omega}_\alpha = \sum_{\lambda=1}^{N_\mathrm{R}} k_\lambda (\nu_{\alpha\lambda}^{(\mathrm{p})} - \nu_{\alpha\lambda}^{(\mathrm{r})}) \prod_{\alpha=1}^{N_\mathrm{S}} c_\alpha^{\nu_{\alpha\lambda}^{(\mathrm{r})}} \quad . \tag{6}$$

Herein $\nu_{\alpha\lambda}^{(\mathrm{r})}$ and $\nu_{\alpha\lambda}^{(\mathrm{p})}$ denote the stoichiometric coefficients of reactants and products respectively and $c_\alpha$ is the concentration of the species $\alpha$. The rate coefficients $k_\lambda$ of the elementary reactions are given by a modified Arrhenius law

$$k_\lambda = A_\lambda T^{\beta_\lambda} \exp\left( -\frac{E_{\mathrm{a}\lambda}}{RT} \right) \quad . \tag{7}$$

The parameters $A_\lambda$, $\beta_\lambda$ of the pre-exponential factor and the activation energy $E_{\mathrm{a}\lambda}$ are determined by a comparison with experimental data[2]. A detailed mechanism with 37 elementary reactions among 9 species by Maas and Warnatz[9] has been used to describe the chemical kinetics of the $H_2/O_2/N_2$ system. The methane-air mechanism employed for the DNS presented in Sect. 6 comprising 84 elementary reactions among 15 species is based on that of Smooke[10]. Besides the computation of the reaction kinetics, detailed models are also utilized for the computation of the thermodynamical properties, the viscosity and the molecular and thermal diffusion velocities[11,2]. These equations are complemented by a state equation, generally the ideal gas law

$$p = \frac{\varrho}{\overline{M}} RT \tag{8}$$

with $R$ being the gas constant and $\overline{M}$ the mean molar mass of the mixture.

## 3 Structure and Performance of the Parallel Code

A code has been developed for the DNS of reactive flows using detailed models for chemical kinetics and molecular transport as described in the last section. This code has been designed for parallel computers with distributed memory like the Cray T3E as the target platform[12, 7]. As at least parameter studies using DNS with detailed chemistry and transport in three spatial dimensions are computationally prohibitive, we restrict ourselves to two spatial dimensions. As turbulence is an inherently three-dimensional phenomenon this is a serious drawback. Nevertheless, we consider the inclusion of a realistic description of chemical reactions and molecular transport to be at least as important as an extension to three dimensions.

The spatial discretization in this code is performed using a finite-difference scheme with sixth-order central-derivatives, avoiding numerical dissipation and leading to very high accuracy. Depending on the boundary conditions, lower order schemes are used at the outermost grid points. The integration in time is carried out using a fourth-order fully explicit Runge-Kutta method. The time step of the integration is controlled by three different limiting conditions. A Courant-Friedrichs-Lewy (CFL) criterion and a Fourier criterion for the diffusion terms are checked to ensure the stability of the integration. An additional accuracy control of the solution is obtained through time-step doubling.

The parallelization strategy is based on a regular two-dimensional domain decomposition with a three points wide region of halo elements at the domain boundaries. Using these locally stored values, an integration step on each subdomain is carried out independently from the other nodes. After each integration step, the new inner boundary values of the subdomain are sent to and the new values of the surrounding region are received from the neighbouring nodes via message-passing communication.

Below, we present performance results for the Cray T3E optimized implementation of our code using MPI as message-passing library. All computations have been performed on Cray T3E-900 systems, i.e. $450\,\mathrm{MHz}$ clock speed and stream buffers enabled. Having access to a node with 512 MB RAM allows us to perform a one-processor reference computation for the $H_2/O_2/N_2$ system with $544 \times 544$ grid points, a problem size which corresponds to some real production runs. The achieved speedups and efficiencies for this benchmark are given in Table 1. An average rate of $86.3$ MFlop/s per PE is achieved in this computation using 64 processors[13].

The classical parallel efficiency for a problem of fixed size as given above obviously includes the loss due to the overhead for communication and synchronization as well as differences caused by the decreasing load per processor. (Of course the amount of data which has to be sent to and received from other processors is also decreasing in this case.) An alternative measure is the scaled parallel efficiency, i. e. the ratio of the computing time for solving an problem of the size $p \cdot N$ using $p$ processors and the computing time for

| processors | 1 | 4 | 8 | 16 | 32 | 64 | 128 | 256 | 512 |
|---|---|---|---|---|---|---|---|---|---|
| speedup | 1 | 4.3 | 8.1 | 15.9 | 30.5 | 57.9 | 108.7 | 189.0 | 293.6 |
| efficiency | 100.0 | 106.6 | 100.7 | 99.2 | 95.3 | 90.4 | 84.9 | 73.8 | 57.4 |

Table 1. Scaling on a Cray T3E for a DNS with 9 species and 37 reactions on a $544^2$ points grid

solving the corresponding problem of size $N$ on one processor. Choosing a constant load per processor of $32^2$ grid points and the chemical mechanism for the hydrogen-air system, a scaled parallel efficiency of $76.8\,\%$ has been achieved using 256 PEs of a Cray T3E-900.

One of the most time-consuming parts in DNS like those presented in the following sections is the computation of the chemical source terms on the right-hand sides of the species-mass conservation equations by evaluating Eq. (6). In several cases of interest, a vast reduction of this time can be achieved without a significant loss in accuracy by using an adaptive evaluation of the chemical source terms. A dynamic load-balancing procedure is used in the parallel adaptive computations to maintain a high efficiency. This method is described in detail in Ref. 14 for non-premixed turbulent combustion and has been extended to premixed turbulent flames as described in Ref. 15.

## 4 Autoignition in a Turbulent Mixing Layer

Autoignition takes place in combustion systems like Diesel engines, in which fuel ignites after being released into a turbulent oxidant of elevated temperature. The influence of the turbulent flow field on the ignition-delay time and the spatial distribution of ignition spots is studied in a model configuration shown in Fig. 1. A cold fuel stream in the left of the computational domain and an air stream with an elevated initial temperature in the right half of the computational domain are superimposed with a turbulent flow field computed by inverse FFT from a von-Kármán-Pao-spectrum with randomly chosen phases. Non-reflecting outflow conditions[16] are used at the boundaries in $x$-direction and periodic boundary conditions are used in $y$-direction. In the simulation presented here, the fuel stream consists of $10\,\%$ hydrogen and $90\,\%$ nitrogen (mole fractions) at a temperature of $T_1 = 298\,\mathrm{K}$ and the initial temperature of the air stream is $T_2 = 1100\,\mathrm{K}$. The Reynolds number of the turbulent flow field based on the integral length scale is $\mathrm{Re}_\Lambda(t_0) = 252$.

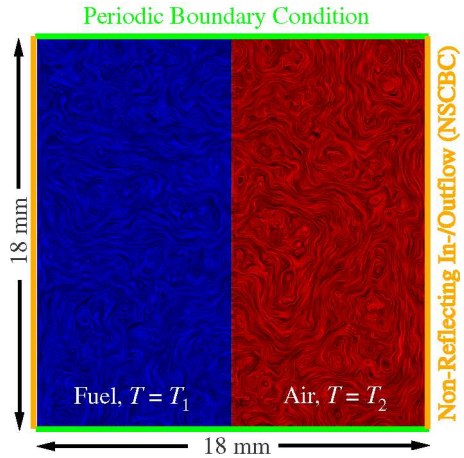


Figure 1. Initial conditions for the DNS of autoignition in a turbulent mixing layer

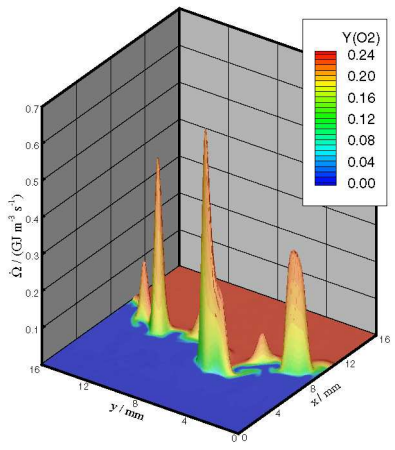


Figure 2. Ignition spots at the time of strongest increase of maximum heat release rate

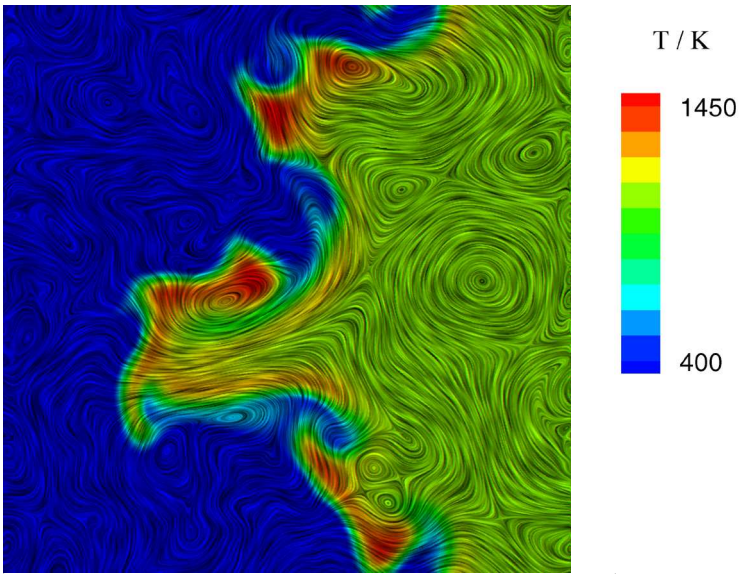


Figure 3. Snapshot of the flow field and temperature distribution in a turbulent reactive mixing layer

After a specific temporal delay, which is characteristic for chemical reactions which are governed by a chain-branching mechanism, a very fast increase of the heat release rate $\dot{\Omega}$ in distinct spatial regions is observed. Fig. 2 shows these ignition spots for one such simulation. The flow field visualized by line integral convolution[17] after one millisecond is shown in Fig. 3 while the colors mark the temperature, which has risen up to $T_{\max}(\vec{x}, t_0 + 1\,\mathrm{ms}) = 1549\,\mathrm{K}$ due to the heat released in the flame front.

Main results of these DNS regard the influence of turbulence on the ignition delay time and the spatial occurence of the ignition spots[5]. For the latter problem, it has been shown analytically using simplified models that in the corresponding laminar situation autoignition takes place at the coordinate where the mixture fraction has a specific value[18]. The ignition spots in the DNS of turbulent mixing layers also appear along isolines of the mixture fraction. As in the laminar case, the specific value of the most reactive mixture fraction depends on the temperatures and chemical compositions of the fuel and oxidizer streams. The curvature of the mixture-fraction isolines has been identified as an additional parameter determining the spatial location of the ignition spots. In regions with curvature being convex towards the fuel side, the focussing of the faster diffusing species like atomic hydrogen increases their concentration on the hot fuel-lean side of the mixing layer. Obviously, it would not have been possible to identify this effect using an oversimplified model for chemical kinetics or a description of the transport omitting differential diffusion.

## 5 Induced Ignition of a Turbulent Hydrogen-Air Mixture

Induced ignition is another phenomenon of practical importance, e. g. in Otto engine combustion and safety considerations. DNS studies of this process have been performed using

simple one-step chemistry in a model configuration of an initially uniform premixed gas under turbulent conditions which is ignited by an energy source[19]. The same configuration has been used for the detailed chemistry DNS presented here. A cold ($T = 298\,\mathrm{K}$) hydrogen-air mixture is superimposed with a turbulent flow field. During the first $15\,\mu\mathrm{s}$ of the simulation an energy-source in a small circular region at the center of the computational domain is active. During this time the mixture at the center of the domain heats up, radicals are formed, and the mixture ignites. A shockwave is observed which propagates outwards towards the boundaries of the domain. Non-reflecting outflow conditions based on characteristic wave relations[16] are imposed on all boundaries to allow the shock wave to leave the domain without disturbing the solution. Above a minimum ignition energy an expanding flame kernel is observed.

Figure 4 shows the temporal evolution of such a flame kernel in the turbulent flow field after the ignition. The first row of images shows the mass fraction of $H_2O_2$, a radical which is confined to a very thin layer in the flame, at $t = 0.2\,\mathrm{ms}$, $t = 0.4\,\mathrm{ms}$, and $t = 0.6\,\mathrm{ms}$, respectively. Below, the temporal evolution of vorticity is shown. The lack of a vortex-stretching mechanism in two-dimensional simulations of decaying turbulence leads to an inverse cascade with growing structures. There is a very strong damping of the turbulence in the hot region of the burnt gas due to the high viscosity. A comparison shows a good qualitative agreement of the DNS presented with the results of an experimental investigation of turbulent flames performed under similar conditions[20].

A quantitative analysis requires specialized tools for the postprocessing of the large and complex datasets generated by DNS. An extensible tool has been developed which allows to extract several features from these datasets. This is illustrated in Figs. 5 and 6 which exemplify results gained from the simulation of the turbulent flame kernel shown

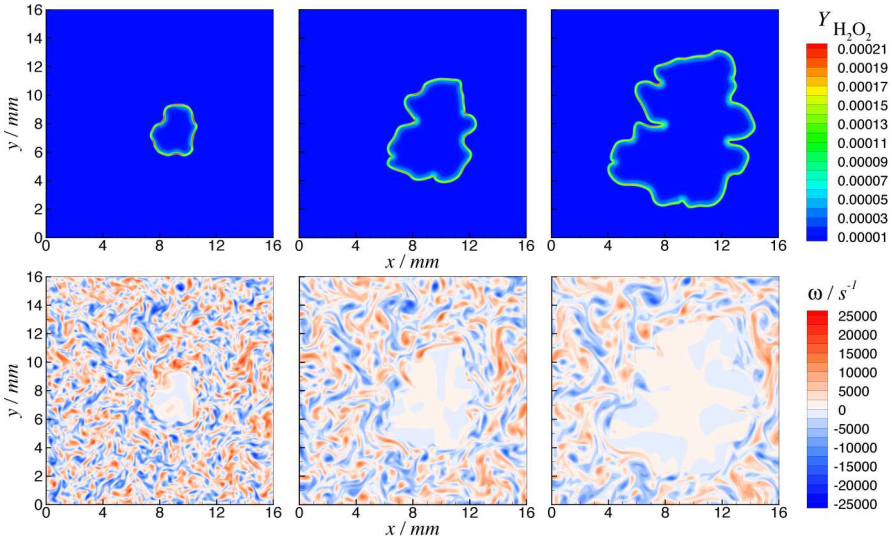


Figure 4. $H_2O_2$ mass fraction (top) and vorticity (bottom) at $t = 0.2\,\mathrm{ms}$, $t = 0.4\,\mathrm{ms}$, and $t = 0.6\,\mathrm{ms}$ (left to right) in a turbulent flame kernel evolving after induced ignition.

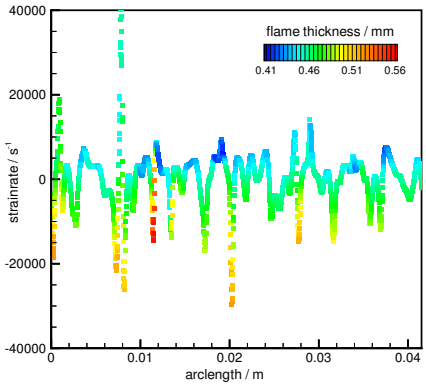


Figure 5. Strain rate and flame thickness along the front of the flame shown in Fig. 4 at $t = 0.6\,\mathrm{ms}$

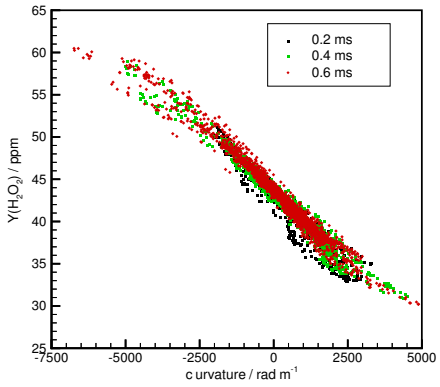


Figure 6. Correlation of $H_2O_2$ mass fraction and flame front curvature

in Fig. 4. In Fig. 5 the strain rate and the flame thickness (based on the local temperature gradient) along the flame front at $t = 0.6\,\mathrm{ms}$ are shown. The correlation of the $H_2O_2$ mass fraction and the curvature of the flame is shown in Fig. 6 for subsets of the DNS data with $T = (T_{\mathrm{max}} + T_{\mathrm{min}})/2 = 1140\,\mathrm{K}$. High concentrations of the $H_2O_2$ radical in the reaction zone evidently occur in regions with high negative curvature, i. e. convex towards the burnt gas. Such changes of the chemical composition in curved flame fronts are caused by preferential diffusion[21,22].

## 6 Turbulent Premixed Methane Flame

The structure and propagation of turbulent flames has also been studied by DNS of the temporal evolution of an initially planar flame in a turbulent flow field[23,5]. A snapshot of such an synthetic turbulent premixed methane-air flame is shown in Fig. 7. The third coordinate direction is used here to visualize the fuel mass fraction $Y_{\mathrm{CH_4}}$ where the contour colors denote the mass fraction of OH which is an important intermediate radical. The initially flat flame has been interacting with the turbulent flow field for $1.35\,\mathrm{ms}$ which is about $1.8$ times the large-eddy turnover time $t_\Lambda$. An interesting phenomenon to be seen in Fig. 7 is the isolated pocket of cold unburnt fuel which has propagated into the hot burnt gas side of the flame. The occurence of such pockets in turbulent flames is well known from experiments[24]. The transient process of pocket formation involves mutual annihilation of parts of the flame front and is discussed and shown in more detail in Refs. 23, 25 for the case of hydrogen flames.

Figure 8 shows the spatial distribution of the local heat release rate in the same turbulent flame at the same time as shown in Fig. 7. The main heat release occurs inside a thin layer with strong variations along the flame front which are mainly determined by the curvature of this reaction layer. The local heat release rate is one of the most important properties of turbulent flames with respect to turbulent combustion modeling. The direct experimental measurement of the heat release rate is extremely difficult, if not impossible. The only practical approach is to measure some other quantity that has some correlation

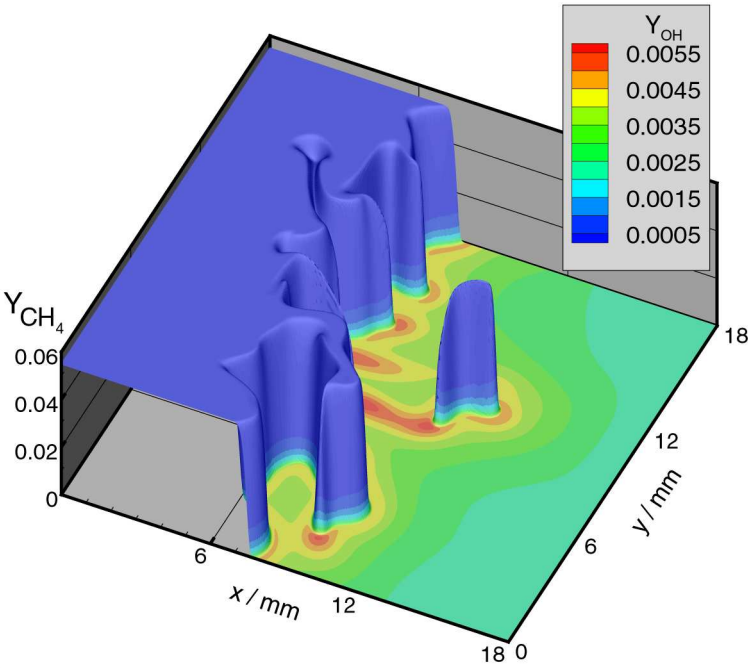


Figure 7. Snapshot of fuel (height) and OH (colors) mass fractions in a turbulent premixed methane-air flame

with this rate over the relevant range of flame and flow parameters[26]. It is e. g. possible to perform spatially resolved measurements of concentrations of trace species like OH, CH, and HCO. An extremely useful result is therefore the fact that the local heat release rate is very well correlated with the HCO concentration as can be seen in Fig. 9. This holds for

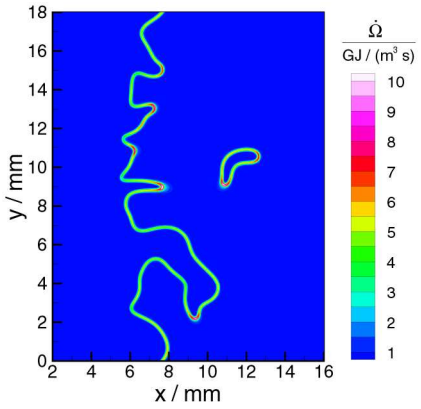


Figure 8. Heat release rate in a turbulent premixed methane-air flame at $t = 1.8\,t_\Lambda$

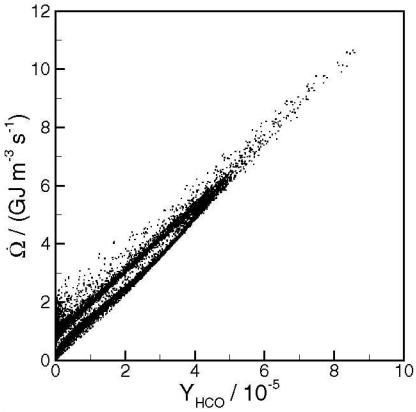


Figure 9. Correlation of local heat release rate with HCO mass fraction

the complete temporal evolution and also for methane-air flames with different equivalence ratios and for varied turbulence intensity.

## 7 Conclusion

A code for the DNS of turbulent reactive flows using detailed models for chemical kinetics and molecular transport has been presented. This code exhibits good performance and an excellent scaling behaviour on Cray T3E systems. It has been used to study non-premixed and premixed turbulent combustion processes in several configurations. Exemplary application results presented in this paper regard the influence of turbulence on autoignition in a mixing layer, the structure of a flame kernel evolving after induced ignition of a turbulent hydrogen-air mixture, and pocket formation in a premixed methane-air flame propagating in a turbulent flow field. In this last case, a correlation analysis reveals the suitability of HCO as a trace species for the heat release rate. Making use of adaptive techniques like the adaptive evaluation of chemical source terms mentioned in Sect. 3 and harnessing the power of modern supercomputers will remain to be of key importance for future DNS. The ongoing increase of computational power available will further strengthen the usage of DNS as a tool in combustion research.

## Computational Resources

All presented DNS have been performed using the Cray T3E systems of the John von Neumann Institute for Computing at Jülich (NIC) and of the High-Performance Computing Center at Stuttgart (HLRS). The CPU-time for individual DNS depends on several parameters including the size of the computational grid, the number of chemical species and elementary reactions considered, the physical time for which the temporal evolution is computed, the achievable timesteps for the integration, etc.. A good example for a typical production run is the DNS of a turbulent reactive mixing layer as presented in Sect. 4 up to a physical time of one milisecond on an $800 \times 800$ points grid. Using 256 PEs of the Cray T3E-1200 this computation took about 23 hours. Our study of this configuration includes several such DNS in which parameters like turbulence intensity and the initial temperature of the air stream have been varied.

## References


1. K. N. C. Bray, *The Challenge of Turbulent Combustion*, Proceedings of the Combustion Institute **26**, 1–26 (1996).
2. J. Warnatz, U. Maas, R. W. Dibble, *Combustion*, 2nd edn., Springer (1999).
3. T. J. Poinsot, *Using Direct Numerical Simulations to Understand Premixed Turbulent Combustion*, Proceedings of the Combustion Institute **26**, 219–232 (1996).
4. T. Mantel and J.-M. Samaniego, *Fundamental Mechanisms in Premixed Turbulent Flame Propagation via Vortex-Flame Interactions, Part II: Numerical Simulation*, Combustion and Flame **118**, 557–582 (1999).
5. M. Lange and J. Warnatz, *Investigation of Chemistry-Turbulence Interactions Using DNS on the Cray T3E*, High Performance Computing in Science and Engineering '99, E. Krause and W. Jäger (Eds.), 333–343, Springer (2000).

6. M. Baum, *Performing DNS of Turbulent Combustion with Detailed Chemistry on Parallel Computers*, Parallel Computing: Fundamentals, Applications and New Directions, E. D'Hollander et al. (Eds.), 145–153, Elsevier (1998).
7. M. Lange, D. Thévenin, U. Riedel, and J. Warnatz, *Direct Numerical Simulation of Turbulent Reactive Flows Using Massively Parallel Computers*, Parallel Computing: Fundamentals, Applications and New Directions, E. D'Hollander et al. (Eds.), 287–296, Elsevier (1998).
8. R. B. Bird, W. E. Stewart, E. N. Lightfoot, *Transport Phenomena*, Wiley (1960).
9. U. Maas and J. Warnatz, *Ignition Processes in Hydrogen-Oxygen Mixtures*, Combustion and Flame **74**, 53–69 (1988).
10. M. D. Smooke, R. Mitchell, D. E. Keyes, *Numerical Simulation of Two-Dimensional Axisymmetric Laminar Diffusion Flames*, Combustion Science and Technology **67**, 85–122 (1989).
11. R. Kee, et al., *A Fortran Computer Code Package for the Evaluation of Gas-Phase Multicomponent Transport Properties*, Sandia National Laboratories Report SAND86-8246 (1986).
12. D. Thévenin, et al., *Development of a Parallel Direct Simulation Code to Investigate Reactive Flows*, Computers and Fluids **25**(5), 485–496 (1996).
13. M. Lange and J. Warnatz, *Direct Simulation of Turbulent Reacting Flows on the Cray T3E*, Proceedings of the 14th Supercomputer Conference '99 in Mannheim, H.-W. Meuer (Ed.) (1999).
14. M. Lange, *Parallel DNS of Autoignition Processes with Adaptive Computation of Chemical Source Terms*, Parallel Computational Fluid Dynamics: Trends and Applications, C. Jenssen, et al. (Eds.), 551–558, Elsevier (2001).
15. M. Lange, *Adaptive Chemistry Computation to Accelerate Parallel DNS of Turbulent Combustion*, High Performance Computing in Science and Engineering 2000, E. Krause and W. Jäger (Eds.), 412–424, Springer (2001).
16. M. Baum, T. J. Poinsot, D. Thévenin, *Accurate Boundary Conditions for Multicomponent Reactive Flows*, Journal of Computational Physics **116**, 247–261 (1995).
17. D. Stalling and H.-C. Hege, *Fast and Resolution Independent Line Integral Convolution*, Proceedings of the 22nd annual ACM conference on computer graphics, 249–256 (1995).
18. A. Liñan and A. Crespo, *An Asymptotic Analysis of Unsteady Diffusion Flames for Large Activation Energies*, Combustion Science and Technology **14**, 95–117 (1976).
19. T. Echekki, T. J. Poinsot, T. A. Baritaud, and M. Baum, *Modeling and Simulation of Turbulent Flame Kernel Evolution*, Transport Phenomena in Combustion, S. H. Chan (Ed.), Vol. 2, 951–962, Taylor & Francis (1995).
20. B. Renou, A. Boukhalfa, D. Puechberty, and M. Trinité, *Local Scalar Flame Properties of Freely Propagating Premixed Turbulent Flames at Various Lewis Numbers*, Combustion and Flame **123**, 507–521 (2000).
21. C. K. Law, *Dynamics of Stretched Flames*, Proceedings of the Combustion Institute **22**, 1381–1402 (1988).
22. M. Lange and J. Warnatz, *A DNS Study of Curvature Effects in Turbulent Premixed Flames*, Scientific Computing in Chemical Engineering II, F. Keil et al. (Eds.), Vol. 2: Simulation, Image Processing, Optimization, and Control, 126–133, Springer (1999).
23. M. Lange, U. Riedel, J. Warnatz, *Parallel DNS of Turbulent Flames with Detailed*

*Reaction Schemes*, AIAA Paper 98-2979 (1998).
24. F. Baillot and A. Bourhela, *Burning Velocity of Pockets from a Vibrating Flame Experiment*, Combustion Science and Technology **126**, 201–224 (1997).
25. M. Lange and J. Warnatz, *Detailed Simulations of Turbulent Flames Using Parallel Supercomputers*, High Performance Computing in Science and Engineering '98, E. Krause and W. Jäger (Eds.), 343–352, Springer (1999).
26. H. N. Najm, P. H. Paul, C. J. Mueller, P. S. Wyckhoff, *On the Adequacy of Certain Experimental Observables as Measurements of Flame Burning Rate*, Combustion and Flame **113**, 312–332 (1998).